

Impact of decoherence on the metrological advantage of weak-value amplification

Yu-Han Yan(严雨涵), Yan-Ping Tan(谭艳萍), Yan-Yan Lu(陆艳艳), Shao-Jie Xiong(熊少杰), and Zhe Sun(孙哲)

Citation: Chin. Phys. B, 2026, 35 (**1**): 010307. DOI: 10.1088/1674-1056/ae29fe
http://cpb.iphy.ac.cn; http://iopscience.iop.org/cpb

What follows is a list of articles you may be interested in

Observation of topology of non-Hermitian systems without chiral symmetry

Shuo Wang(王硕), Zhengjie Kang(康正杰), Hao Li(李浩), Jiaojiao Li(李姣姣), Yuanjie Zhang(张元杰), and Zhihuang Luo(罗智煌)

Chin. Phys. B, 2025, 34 (**11**): 110304. DOI: 10.1088/1674-1056/addcc1

Exceptional rings and non-Abelian topology in non-Hermitian high-spin systems

Peng-Zhen Sun(孙鹏震), Zhou-Tao Lei(雷周涛), and Yuan-Gang Deng(邓元刚)

Chin. Phys. B, 2025, 34 (**11**): 110303. DOI: 10.1088/1674-1056/addcbe

Optimal multi-parameter quantum metrology for frequencies of magnetic field

Zhenhua Long(龙振华) and Shengshi Pang(庞盛世)

Chin. Phys. B, 2025, 34 (**8**): 080301. DOI: 10.1088/1674-1056/add4e7

Quantum-enhanced time-of-arrival measuring method based on partially entangled state

Peng-Xian Li(李芃鲜), Lu-Ping Xu(许录平), Gui-Ting Hu(胡桂廷), and Wen-Long Gao(高文珑)

Chin. Phys. B, 2025, 34 (**7**): 070303. DOI: 10.1088/1674-1056/adc7ee

Sudden change of interferometric power for X-shape states

Dian Zhu(朱典), Fu-Lin Zhang(张福林), and Jing-Ling Chen(陈景灵)

Chin. Phys. B, 2025, 34 (**2**): 020305. DOI: 10.1088/1674-1056/ad9732

Impact of decoherence on the metrological advantage of weak-value amplification

Yu-Han Yan(严雨涵)[2,†], Yan-Ping Tan(谭艳萍)[1,†], Yan-Yan Lu(陆艳艳)[1,‡], Shao-Jie Xiong(熊少杰)[1,§], and Zhe Sun(孙哲)[1,¶]

[1] *College of Big Data and Intelligent Engineering, Guizhou University of Commerce, Guiyang* 550014, *China*
[2] *School of Physics, Hangzhou Normal University, Hangzhou* 310036, *China*

(Received 6 October 2025; revised manuscript received 13 November 2025; accepted manuscript online 9 December 2025)

We present a theoretical investigation of weak-value amplification (WVA) under decoherence, quantifying its metrological capabilities through the quantum Fisher information (QFI). By modeling decoherence via Kraus operators acting before and after the weak measurement interaction, we derive exact expressions for the QFI governing parameter estimation of a weak coupling strength. These analytical results reveal the fundamental limitation imposed by decoherence on the QFI achievable via WVA. From these results, the optimal post-selection state that maximizes the QFI can be derived for different noise environments. Through paradigmatic examples, including amplitude damping and depolarizing channels, we demonstrate a key distinction: the optimal post-selection evolves with the noise strength in the amplitude damping channel, but is fixed in the depolarizing channel. This work provides both theoretical insights and practical guidance for optimizing metrological schemes based on WVA in realistic decoherent environments.

Keywords: quantum metrology, weak-value amplification, quantum Fisher information

PACS: 03.65.Ta, 03.65.Yz

DOI: 10.1088/1674-1056/ae29fe **CSTR:** 32038.14.CPB.ae29fe

1. Introduction

The pursuit of ultimate precision in parameter estimation has given rise to the field of quantum metrology. This field leverages uniquely quantum-mechanical resources — such as entanglement, squeezing effects, and quantum coherence — to surpass classical fundamental limits.[1–3] A key focus of this effort is the quantum Fisher information (QFI), which quantifies the maximum amount of information that a quantum state carries about an unknown parameter and sets a lower bound on the estimation uncertainty via the quantum Cramér–Rao inequality.[4,5] Consequently, maximizing the QFI is a central goal in the design of advanced quantum measurement schemes.

Among the various strategies for parameter estimation, the technique of weak-value amplification (WVA) has attracted significant theoretical and experimental interest since its introduction by Aharonov, Albert, and Vaidman.[6] The WVA protocol involves a weak unitary interaction, generated by a Hamiltonian coupling the system to a meter. By employing a proper pre-selection of the initial system state and a post-selection onto a nearly orthogonal final state, the protocol can produce an anomalously large weak value for the system. This amplified weak value effectively enhances the QFI associated with the estimated parameter.[7,8] Although this comes at the cost of a reduced sample size, the amplified QFI can lead to improved precision under practical constraints, such as detector saturation or dominant technical noise.[9,10]

This amplification mechanism has been successfully applied in numerous experimental contexts to enhance the sensitivity of measuring small physical effects.[11,12] Notable applications include the precise measurement of ultrasmall beam deflections,[13] frequency shifts,[14] phase shifts,[15,16] and velocity estimation.[17] The practical utility of WVA continues to be a rich subject of investigation, exploring its advantages in signal-to-noise ratio and its robustness against certain types of noise. However, a primary challenge in any quantum-enhanced technology is its susceptibility to decoherence — the loss of quantum coherence due to inevitable interactions with a surrounding environment.[18–20] Decoherence typically causes a rapid degradation of fragile quantum resources such as entanglement and coherence, which are essential for both standard quantum metrology and WVA.[21–23] Decoherence at any stage of the WVA process (before, during, or after the weak interaction) can severely undermine both the information gain and the apparent amplification advantage. Therefore, a comprehensive understanding of how decoherence impacts the ultimate precision limit — as quantified by the QFI — is not only of theoretical interest but also crucial for assessing

[†]These authors contributed equally to this work.
[‡]Corresponding author. E-mail: xiaoguai@gzsxy361.wecom.work
[§]Corresponding author. E-mail: 202410003@gzcc.edu.cn
[¶]Corresponding author. E-mail: sunzhe@hznu.edu.cn

© 2026 Chinese Physical Society and IOP Publishing Ltd. All rights, including for text and data mining, AI training, and similar technologies, are reserved.

the practicality of WVA-based sensors.

Our analysis reveals how decoherence fundamentally limits the achievable precision, and thereby constrains the amplification advantage. Furthermore, our analytical results demonstrate that the optimal post-selection state is highly dependent on the specific decoherence model. For instance, it undergoes significant changes with increasing decoherence strength in the amplitude damping (AD) channel, whereas it remains unchanged under the isotropic depolarizing channel. This understanding serves to optimize practical quantum sensors operating in noisy environments.

2. Parameter estimation via weak value amplification

A schematic of the WVA under local decoherence is depicted in Fig. 1. The procedure begins with the meter and the system initialized in a product state, formulated as $|\Psi_i\rangle = |\psi_{si}\rangle|\phi_{mi}\rangle$. From the initial time $t_0 = 0$, the system is subject to a local decoherence process due to a Markovian system–environment coupling, lasting until time t_1 before the weak interaction. This decoherence evolves the initial pure product state into a mixed state, described as

$$\rho_{s,m} = \sum_n (K_{t_1,n} \otimes \mathbb{I}_m)|\Psi_i\rangle\langle\Psi_i|(K_{t_1,n}^\dagger \otimes \mathbb{I}_m), \tag{1}$$

where $\{K_{t_1,n}\}$ are the Kraus operators acting solely on the system, satisfying $\sum_n K_{t_1,n}^\dagger K_{t_1,n} = \mathbb{I}_s$. Then, at time t_1, the system and meter interact via an impulsive Hamiltonian $H_I(t) = g\delta(t-t_1)AM$, where A and M are the operators acting on the system and meter, respectively, and g represents the coupling strength, which is also the parameter to be estimated. This form describes an instantaneous unitary operation at time t_1. The unitary parametrization of g can be written as

$$U_g = \exp\left[-\mathrm{i}\int H_I(t)\,\mathrm{d}t\right] = \exp(-\mathrm{i}gAM). \tag{2}$$

This unitary operator U_g evolves the state $\rho_{s,m}^{t_1}$ into

$$\rho_{s,m}^{t_1}(g) = U_g \rho_{s,m}^{t_1} U_g^\dagger. \tag{3}$$

After the weak interaction, the system continues to experience Markovian environmental noise until time t_2. The memoryless nature of this noise allows the second decoherence stage to be consistently modeled by Kraus operators, giving the final state of the system and meter as

$$\rho_{s,m}^{t_2}(g) = \sum_n (K_{t_2,n} \otimes \mathbb{I}_m)\rho_{s,m}^{t_1}(g)(K_{t_2,n}^\dagger \otimes \mathbb{I}_m), \tag{4}$$

where $\{K_{n,t_2}\}$ are the Kraus operators characterizing the second decoherence stage over the time interval $[t_1, t_2]$. Finally, a projective measurement $|\psi_{sf}\rangle\langle\psi_{sf}|$ is performed on the system and the collapsed state of the meter is given by

$$\rho_m^{t_2}(g) = \frac{1}{p}\langle\psi_{sf}|\rho_{s,m}^{t_2}(g)|\psi_{sf}\rangle, \tag{5}$$

with $p = \mathrm{Tr}\left(\langle\psi_{sf}|\rho_{s,m}^{t_2}(g)|\psi_{sf}\rangle\right)$. For the quantum state $\rho_m^{t_2}(g)$, the ultimate precision limit for unbiased estimation of parameter g via ν repeated measurements is given by the quantum Cramér–Rao bound

$$\langle(g - g_{est})^2\rangle \geq \frac{1}{\nu\mathcal{F}}, \tag{6}$$

where g_{est} is the unbiased estimator for g, $\mathcal{F}$ is the QFI, defined by[1,24]

$$\mathcal{F} = \mathrm{Tr}\left[\rho_m^{t_2}(g)L_g^2\right], \tag{7}$$

where the symmetric logarithmic derivative operator L_g is determined implicitly by the equation

$$\frac{\partial\rho_m^{t_2}(g)}{\partial g} = \frac{1}{2}\left[L_g\rho_m^{t_2}(g) + \rho_m^{t_2}(g)L_g\right]. \tag{8}$$

For the weak coupling regime, we expand U_g to the first order, which gives

$$\begin{aligned}&\rho_m^{t_2}(g) \approx \tilde{\rho}_m^{t_2}(g)\\ &= \frac{1}{a}\sum_{n,j}(\mathcal{X}_{n,j}|\phi_{mi}\rangle - \mathrm{i}g\mathcal{Y}_{n,j}M|\phi_{mi}\rangle)\cdot\left(\langle\phi_{mi}|\mathcal{X}_{n,j}^* + \mathrm{i}g\langle\phi_{mi}|M\mathcal{Y}_{n,j}^*\right),\end{aligned} \tag{9}$$

where $\mathcal{X}_{n,j} = \langle\psi_{sf}|K_{n,t_2}K_{j,t_1}|\psi_{si}\rangle$, $\mathcal{Y}_{n,j} = \langle\psi_{sf}|K_{n,t_2}AK_{j,t_1}|\psi_{si}\rangle$, $a = \sum_{n,j}|\mathcal{X}_{n,j}|^2 + g^2\langle M^2\rangle_i\sum_{n,j}|\mathcal{Y}_{n,j}|^2$. We assume that the initial meter state satisfies $\langle\phi_{mi}|M|\phi_{mi}\rangle = 0$. This standard choice ensures that the meter's response is dominated by the effective parameter-estimation term arising from the weak interaction. Under this condition, the QFI for the quantum state $\tilde{\rho}_m^{t2}(g)$ can be calculated in the two-dimensional subspace spanned by the orthonormal basis vectors $|\phi_{mi}\rangle$, $M|\phi_{mi}\rangle/\langle M^2\rangle_i^{1/2}$. Within the Bloch representation associated with this basis, the QFI can be expressed as[25]

$$\mathcal{F} = \begin{cases}|\partial_g\boldsymbol{\omega}|^2, & (g=0),\\ |\partial_g\boldsymbol{\omega}|^2 + \dfrac{(\boldsymbol{\omega}\cdot\partial_g\boldsymbol{\omega})^2}{1-|\boldsymbol{\omega}|^2}, & (g\neq 0),\end{cases} \tag{10}$$

where $\boldsymbol{\omega} = [\mathrm{Tr}(\tilde{\sigma}_x\tilde{\rho}_m(g))\ \ \mathrm{Tr}(\tilde{\sigma}_y\tilde{\rho}_m(g))\ \ \mathrm{Tr}(\tilde{\sigma}_z\tilde{\rho}_m(g))]$ is the effective Bloch vector constructed in the two-dimensional subspace spanned by $|\phi_{mi}\rangle$ and $M|\phi_{mi}\rangle/\langle M^2\rangle_i^{1/2}$, with $\tilde{\sigma}_x, \tilde{\sigma}_y, \tilde{\sigma}_z$ being the Pauli operators defined in this projected space. The explicit form of the QFI for the meter state $\tilde{\rho}_m^{t_2}(g)$ is derived as follows:

$$\mathcal{F}(\tilde{\rho}_m^{t_2}(g)) = \frac{4\left|\sum_{n,j}\mathcal{X}_{n,j}\mathcal{Y}_{n,j}^\dagger\right|^2}{\left(\sum_{n,j}|\mathcal{X}_{n,j}|^2\right)^2}\langle M^2\rangle_i, \quad (g=0), \tag{11}$$

$$\mathcal{F}(\tilde{\rho}_m^{t_2}(g)) \approx \frac{4Y}{X}\langle M^2\rangle_i, \quad (g\neq 0\ \&\ g\ll 1), \tag{12}$$

where $Y = \sum_{n,j}|\mathcal{Y}_{n,j}|^2$ and $X = \sum_{n,j}|\mathcal{X}_{n,j}|^2$.

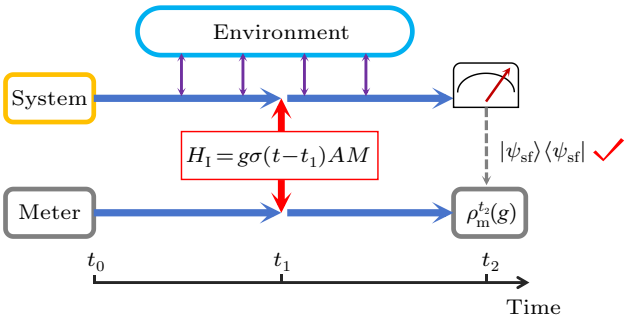


Fig. 1. Temporal diagram of the WVA process under local decoherence. The process begins at t_0 with the initialization of the system and meter. From t_0 to t_1, the system undergoes the first decoherence stage due to interaction with the environment. At time t_1, a weak unitary interaction $H_I = g\delta(t-t_1)AM$ couples the system and meter. This is followed by the second decoherence stage until time t_2. The process concludes with a projective measurement on the system, yielding the final meter state $\rho_m^{t_2}(g)$.

The validity of this first-order treatment rests on the system operating within the weak coupling regime, which must satisfy two concurrent conditions. First, the perturbative condition $g\sqrt{\langle M^2\rangle_i\langle A^2\rangle_{\rho_s}} \ll 1$ ensures the unitary evolution $U_g \approx \mathbb{I} - igAM$ is accurate, where $\langle A^2\rangle_{\rho_s} = \mathrm{Tr}(\rho_s A^2)$ generalizes the expectation value for the mixed system state after the first decoherence stage. Second, the linear response condition $g^2(Y/X)\langle M^2\rangle_i \ll 1$ guarantees that the amplified signal does not drive the meter beyond its linear response region. The ratio Y/X, modified by decoherence, thus plays a critical role in determining the valid parameter range for the coupling strength g.

In this weak coupling regime, we employ the first-order approximated state $\tilde{\rho}_m^{t_2}(g)$ to calculate the QFI of $\rho_m^{t_2}(g)$. This approach is justified by the local nature of the QFI, which is fundamentally defined through the first-order derivative of the quantum state with respect to the parameter g. Our approximation $\tilde{\rho}_m^{t_2}(g)$ is constructed to match both the true state $\rho_m^{t_2}(g)$ and its first derivative exactly at $g = 0$. Consequently, it yields the exact value for $\mathcal{F}(0)$ at the expansion point. For finite but small values of g, this approximation provides the correct leading-order asymptotic expression for the QFI. Therefore, the QFI of $\rho_m^{t_2}(g)$ can be expressed as

$$\mathcal{F}(\rho_m^{t_2}(g)) = \mathcal{F}(\tilde{\rho}_m^{t_2}(g))\big|_{g=0}, \tag{13}$$

$$\mathcal{F}(\rho_m^{t_2}(g)) = \mathcal{F}(\tilde{\rho}_m^{t_2}(g))\big|_{g\neq 0} + \mathcal{O}_g, \tag{14}$$

where $\mathcal{O}_g$ is the correction of g. There are two distinct expressions for the QFI, corresponding to the cases $g = 0$ and $g \neq 0$ (but $g \ll 1$). This reflects the fundamental difference in the nature of the meter state at the exact point of no coupling ($g = 0$) and in its immediate vicinity ($g \neq 0$). At $g = 0$, the meter remains in its initial pure state, leading to the QFI given by Eq. (13). For any finite g, however weak, the system–meter interaction followed by post-selection prepares the meter in a mixed state, whose asymptotic QFI is captured by the leading term in Eq. (14). The presence of decoherence further accentuates this difference. It is only in the absence of decoherence that both expressions reduce to the standard WVA result. The $g = 0$ case, while mathematically well-defined, is of limited practical utility for parameter estimation since it corresponds to the absence of any coupling to be estimated. Therefore, in the subsequent analysis, we focus exclusively on the $g \neq 0$ regime, which captures the leading-order asymptotic behavior of the QFI for finite but small couplings.

The analytical QFI expression in Eq. (14) is of central importance because it allows us to derive the maximum achievable QFI under generic decoherence and the corresponding optimal post-selection state. This maximum value, which is determined by the ratio of the decoherence-modified transition amplitudes Y and X, characterizes the ultimate precision limit for parameter estimation in WVA-based noisy quantum systems. A key utility of our exact expression is that it provides a direct pathway to identify the optimal post-selection measurement. Mathematically, this optimization problem is maximizing a generalized Rayleigh quotient of the form $\frac{\langle\psi_{sf}|\Omega_A|\psi_{sf}\rangle}{\langle\psi_{sf}|\Omega_I|\psi_{sf}\rangle}$, where $\Omega_A = \sum_{n,j}(K_{n,t_2}AK_{j,t_1})|\psi_{si}\rangle\langle\psi_{si}|(K_{n,t_2}AK_{j,t_1})^\dagger$, $\Omega_I = \sum_{n,j}(K_{n,t_2}K_{j,t_1})|\psi_{si}\rangle\langle\psi_{si}|(K_{n,t_2}K_{j,t_1})^\dagger$. Since Ω_I is positive definite, the maximum value of this quotient corresponds to the largest generalized eigenvalue $\lambda_{\max}$ in $\Omega_A|\psi_{sf}\rangle = \lambda\Omega_I|\psi_{sf}\rangle$, which is equivalent to the standard eigenvalue problem $(\Omega_I^{-1}\Omega_A)|\psi_{sf}\rangle = \lambda|\psi_{sf}\rangle$. For the two-dimensional case under consideration, the eigenvalues satisfy the characteristic equation

$$\lambda^2 - \mathrm{Tr}(\Omega_I^{-1}\Omega_A)\lambda + \det(\Omega_I^{-1}\Omega_A) = 0, \tag{15}$$

and the maximum eigenvalue is explicitly given by

$$\lambda_{\max} = \frac{1}{2}\left[\mathrm{Tr}(\Omega_I^{-1}\Omega_A) + \sqrt{\mathrm{Tr}(\Omega_I^{-1}\Omega_A)^2 - 4\frac{\det(\Omega_A)}{\det(\Omega_I)}}\right]. \tag{16}$$

The optimal post-selection state $|\psi_{sf}^{opt}\rangle = \cos(\frac{\theta^{opt}}{2})|0\rangle + e^{i\phi^{opt}}\sin(\frac{\theta^{opt}}{2})|1\rangle$ is determined by

$$\Omega_A|\psi_{sf}^{opt}\rangle = \lambda_{\max}\Omega_I|\psi_{sf}^{opt}\rangle. \tag{17}$$

In the following sections, we illustrate this procedure through paradigmatic examples of qubit systems subject to AD and depolarizing channels, where the explicit analytical results for both the maximum QFI and the optimal post-selection strategy are derived and analyzed.

3. Qubit system under decoherence channel

3.1. Amplitude damping channel

We consider a scenario where both the system and the meter are two-level quantum systems. The AD channel process acting on the system qubit is described by the Kraus operators

$$K_1 = |0\rangle\langle 0| + \sqrt{r}|1\rangle\langle 1|, \quad K_2 = \sqrt{1-r}|0\rangle\langle 1|, \tag{18}$$

where the damping parameter r satisfies $0 \leq r \leq 1$, and the states $|0\rangle$ and $|1\rangle$ denote the eigenstates of σ_z with eigenvalues $+1$ and -1, respectively. To model the Markovian time evolution of the system under a weak coupling to a zero-temperature environment, the parameter r can be expressed as an exponential decay $r = \mathrm{e}^{-\gamma t}$. This standard form arises from the assumption that the decay rate of the population in the excited state is proportional to the population itself, leading to a simple exponential solution. Here, γ denotes the decay rate, which encapsulates the strength of the coupling to the dissipative environment, and t is the evolution time. We consider the case where the two decoherence time intervals are equal, i.e., $t_1 - t_0 = t_2 - t_1 = t$. The post-selection state on the system is chosen as $|\psi_{\mathrm{sf}}\rangle = \cos(\theta_{\mathrm{f}}/2)|0\rangle + \mathrm{e}^{\mathrm{i}\phi_{\mathrm{f}}}\sin(\theta_{\mathrm{f}}/2)|1\rangle$. The system and meter operators are set to $A = \sigma_z$ and $M = \sigma_x$. The initial states are prepared as $|\psi_{si}\rangle = (|0\rangle + |1\rangle)/\sqrt{2}$ for the system and $|\psi_{\mathrm{m}i}\rangle = |0\rangle$ for the meter. Thus, from Eqs. (14) and (12), the leading-order term of $\mathcal{F}(\rho_{\mathrm{m}}^{t_2}(g))$ can be obtained as

$$\frac{4Y}{X} = \frac{4[2|\alpha|^2(1-r^2) + r^2 - 2r\mathrm{Re}(\alpha\beta^*)]}{2|\alpha|^2 + r^2 + 2r\mathrm{Re}(\alpha\beta^*)}, \tag{19}$$

where $\alpha = \langle 0|\psi_{\mathrm{sf}}\rangle$, $\beta = \langle 1|\psi_{\mathrm{sf}}\rangle$. The optimization problem of maximizing the ratio $4Y/X$ can be formulated as a generalized eigenvalue problem, as defined in Eqs. (16) and (17). Solving this problem yields the maximum value of the leading-order QFI, given by

$$\max\left[\frac{4Y}{X}\right] = 4 \cdot \frac{1 - \frac{r^2}{2} + \frac{1}{2}\sqrt{2-r^2}}{1 - \frac{r^2}{2} - \frac{1}{2}\sqrt{2-r^2}}, \tag{20}$$

which is attained when the post-selection state is the corresponding eigenvector, satisfying $\cos\theta_{\mathrm{sf}}^{\mathrm{opt}} = r^2 - 1$, $\phi_{\mathrm{sf}}^{\mathrm{opt}} = \pi$. This result demonstrates that under the AD channel, the optimal post-selection strategy depends explicitly on the decoherence strength r, with the optimal phase fixed at π, highlighting the substantial role of decoherence in shaping the metrological configuration.

Figure 2(a) displays $\mathcal{F}(\rho_{\mathrm{m}}^{t_2}(g))$ and its leading-order term $4Y/X$ as functions of the post-selection angle θ_{f} (with $\phi_{\mathrm{f}} = 0$) for different values of the coupling strength g and a fixed decoherence rate $\gamma t = 0.5$. As anticipated by our theoretical analysis, the leading-order term exhibits excellent agreement with the exact QFI for small values of g. A detailed comparison of $\mathcal{F}(\rho_{\mathrm{m}}^{t_2}(g))$ and $4Y/X$ as functions of g is provided in Appendix A. This numerical result provides a clear validation of our approximation scheme in the weak coupling regime. The observed convergence between the exact and leading-order QFI as g decreases confirms that our approach correctly provides the asymptotic expression for the QFI in the weak coupling limit.

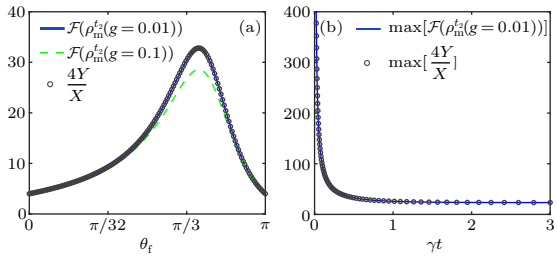


Fig. 2. (a) Under the AD channel, the QFI $\mathcal{F}(\rho_{\mathrm{m}}^{t_2}(g=0.01))$, $\mathcal{F}(\rho_{\mathrm{m}}^{t_2}(g=0.1))$ and the leading-order term $4Y/X$ as functions of the post-selection angle θ_{sf} at $\gamma t = 0.5$ and $\phi_{\mathrm{sf}} = \pi$. (b) The maximum values of $\mathcal{F}(\rho_{\mathrm{m}}^{t_2}(g=0.01))$ and $\max[4Y/X]$ versus γt.

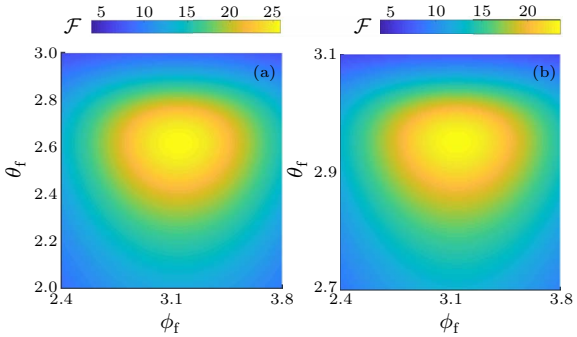


Fig. 3. Under the AD channel, the drift of the optimal post-selection angles with different γt. (a) For $\gamma t = 1$, the optimum occurs at $(\theta_{\mathrm{f}}, \phi_{\mathrm{f}}) = (2.6, \pi)$. (b) For $\gamma t = 2$, the optimum shifts to $(2.95, \pi)$.

Figure 2(b) illustrates the maximum value of $\mathcal{F}(\rho_{\mathrm{m}}^{t_2}(g=0.01))$ and of the leading-order term $4Y/X$ as functions of the decoherence strength γt. For each value of γt, $\max\left[\mathcal{F}(\rho_{\mathrm{m}}^{t_2}(g))\right]$ and $\max\left[4Y/X\right]$ are determined by optimizing the QFI over all possible post-selection angles. A remarkable agreement is observed between these two maxima across the range of γt shown. In the absence of decoherence, the WVA enables a significant enhancement of the QFI, reaching a considerably large value. However, as γt increases, the amplification effect of WVA on the QFI decays rapidly. This behavior clearly demonstrates that environmental decoherence severely diminishes the metrological advantage offered by WVA. The dissipative interaction with the environment causes irreversible information loss, which ultimately limits the maximum achievable precision in parameter estimation.

Decoherence not only reduces the maximum QFI but also shifts the optimal post-selection that attains this maximum. In the absence of decoherence, a significantly enhanced QFI can be achieved through the WVA by choosing a post-selection state that is nearly orthogonal to the initial state, consistent with the standard WVA theory.[26] Figure 3 depicts the dependence of the QFI on the post-selection angles θ_{f} and ϕ_{f} for different decoherence strengths. As γt increases, the location of the maximum QFI in the angular space undergoes a noticeable shift. For instance, when $\gamma t = 1$, the maximum QFI occurs at $\theta_{\mathrm{f}} = 2.6$ and $\phi_{\mathrm{f}} = \pi$; when $\gamma t = 2$, the optimum moves

to $\theta_{\rm f}=2.95$ and $\phi_{\rm f}=\pi$. It is noteworthy that these numerically optimized angles agree remarkably well with the values predicted by our analytical result $\cos\theta_{\rm f}^{\rm opt}=r^2-1$, $\phi_{\rm f}^{\rm opt}=\pi$. This agreement underscores the effectiveness of our analytical framework: it not only clearly reveals the nontrivial interplay between decoherence and measurement optimization — where decoherence changes the functional dependence of the QFI on the post-selection angles — but also provides a quantitative guideline for choosing the optimal post-selection in practical experiments where decoherence is non-negligible.

3.2. Depolarizing channel

The depolarizing channel process acting on the system qubit is described by the Kraus operators

$$K_1=\frac{\sqrt{1+3r}}{2}I,\quad K_2=\frac{\sqrt{1-r}}{2}\sigma_x,$$
$$K_3=\frac{\sqrt{1-r}}{2}\sigma_y,\quad K_4=\frac{\sqrt{1-r}}{2}\sigma_z. \tag{21}$$

Following the same setup as in the AD channel case, we take $A=\sigma_z$, $M=\sigma_x$, and the initial states $|\psi_{si}\rangle=(|0\rangle+|1\rangle)/\sqrt{2}$, $|\psi_{mi}\rangle=|0\rangle$. We also assume that the two decoherence time intervals are equal, i.e., $t_1-t_0=t_2-t_1=t/2$, and that the depolarizing parameter follows the same exponential decay form $r=\mathrm{e}^{-\gamma t}$ for both stages, reflecting the Markovian nature of the noise process. Under the depolarizing channel, the leading-order term of $\mathcal{F}(\rho_{\rm m}^{t_2}(g))$ from Eqs. (14) and (12) is

$$\frac{4Y}{X}=4\cdot\frac{1-2r^2{\rm Re}(\alpha\beta^*)}{1+2r^2{\rm Re}(\alpha\beta^*)}. \tag{22}$$

The corresponding maximum of the leading-order term can be derived by solving the generalized eigenvalue problem defined in Eq. (16). The maximum value is given by

$$\max\left[\frac{4Y}{X}\right]=4\cdot\frac{1+r^2}{1-r^2}, \tag{23}$$

when $\theta_{\rm sf}^{\rm opt}=\pi/2$, $\phi_{\rm sf}^{\rm opt}=\pi$. Figure 4(a) shows the QFI of the exact state $\rho_{\rm m}^{t_2}(g)$ and its leading-order term $4Y/X$ as functions of $\theta_{\rm f}$ ($\phi_{\rm f}=0$) under the depolarizing channel for different values of g at fixed $\gamma t=0.5$. As g decreases, the leading-order term converges to the exact QFI, confirming the accuracy of our first-order approximation. A detailed comparison of $\mathcal{F}(\rho_{\rm m}^{t_2}(g))$ and $4Y/X$ as functions of g is provided in Appendix A. Figure 4(b) plots the maximum values of both $\mathcal{F}(\rho_{\rm m}^{t_2}(g=0.01))$ and the leading-order term $4Y/X$ versus the decoherence strength γt. These two maxima are in perfect agreement and both decrease rapidly with increasing γt.

Figure 5 presents the dependence of $\mathcal{F}(\rho_{\rm m}^{t_2}(g))$ on both $\theta_{\rm f}$ and $\phi_{\rm f}$ for different γt values. Unlike the AD case, the optimal post-selection angles that maximize the QFI remain essentially unchanged at $\theta_{\rm f}=\pi/2$, $\phi_{\rm f}=\pi$ across different depolarization strengths. These numerically optimized angles are in perfect agreement with the analytical results derived from the leading-order expression. This invariance shows a fundamental distinction between the depolarizing and AD channels. The isotropic nature of the depolarizing channel preserves the functional form of the QFI with respect to the post-selection angles as the noise strength increases. Consequently, the optimal measurement basis, determined by the initial system preparation and the observable A, remains fixed, in stark contrast to the noise-dependent drift observed under the directional AD channel.

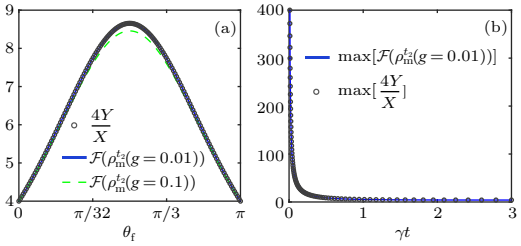


Fig. 4. Under the depolarizing channel, the QFI $\mathcal{F}(\rho_{\rm m}^{t_2}(g=0.01))$, $\mathcal{F}(\rho_{\rm m}^{t_2}(g=0.1))$ and the leading-order term $4Y/X$ as functions of the post-selection angle $\theta_{\rm sf}$ at $\gamma t=0.5$ and $\phi_{\rm sf}=\pi$. (b) The maximum values of $\mathcal{F}(\rho_{\rm m}^{t_2}(g=0.01))$ and $\max[4Y/X]$ versus γt.

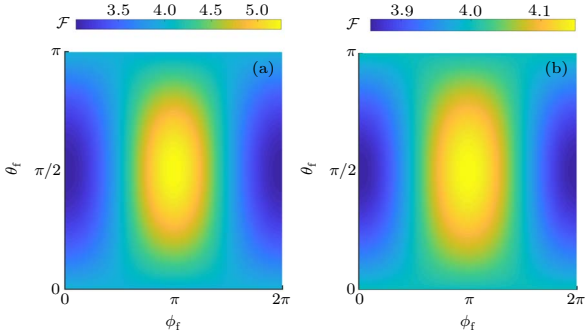


Fig. 5. Under the depolarizing channel, the angles that maximize the QFI remain fixed at $(\theta_{\rm f},\phi_{\rm f})=(\pi/2,\pi)$ for different decoherence strengths: (a) $\gamma t=1$ and (b) $\gamma t=2$.

4. Conclusion

In summary, we have developed a comprehensive theoretical framework to quantify the QFI in WVA under generic local decoherence. By modeling the decoherence process using Kraus operators applied before and after the weak system–meter interaction, we derived exact expressions for the QFI governing the estimation of a weak coupling parameter. Our analysis reveals how environmental decoherence fundamentally limits the QFI and the metrological advantage offered by WVA. Our results provide clear and quantitative guidance for precision measurements based on WVA. Specifically, they demonstrate that to approach the ultimate precision limit under decoherence, an adaptive post-selection strategy must be developed according to the distinct characteristics of the decoherence channel and its strength. The theoretical framework presented here not only deepens the understanding of the interplay between quantum measurements and decoherence but

also offers a practical pathway for optimizing parameter estimation in realistic decoherent quantum systems.

Appendix A

To validate the effectiveness of the analytical approximation and delineate its range of applicability, Fig. A1 compares the exact QFI $\mathcal{F}(\rho_{\mathrm{m}}^{t_2}(g))$ with its leading-order approximation $4Y/X$ as a function of the coupling strength g. The results for the AD channel and the depolarizing channel, with post-selection fixed at their respective optimal angles, are shown in Figs. A1(a) and A1(b), respectively. As demonstrated, the analytical approximation exhibits excellent agreement with the exact numerical results for sufficiently small values of g, thereby providing strong support for all analyses in the main text based on the $g \ll 1$ approximation. A noticeable divergence emerges as g increases, which visually marks the failure boundary of the weak-coupling approximation and corresponds to the violation of the linear response condition $g^2(Y/X)\langle M^2\rangle_i \ll 1$ discussed in the main text.

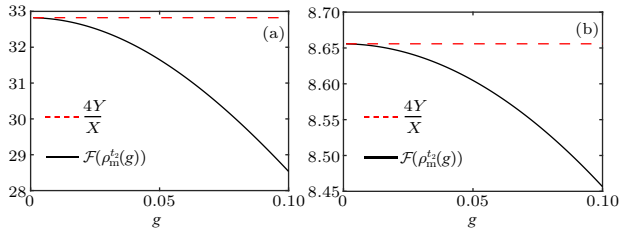


Fig. A1. Comparison between the exact QFI $\mathcal{F}(\rho_{\mathrm{m}}^{t_2}(g))$ and its leading-order analytical approximation $4Y/X$ under decoherence. (a) For the AD channel with a damping parameter $r = \mathrm{e}^{-0.5}$. The post-selection is fixed at the analytically optimized angles $\theta_{\mathrm{f}}^{\mathrm{opt}} = \arccos(r^2-1)$, $\phi_{\mathrm{f}}^{\mathrm{opt}} = \pi$. (b) For the depolarizing channel with a noise parameter $r = \mathrm{e}^{-0.5}$. The post-selection is fixed at its optimal angles $\theta_{\mathrm{f}}^{\mathrm{opt}} = \pi/2$, $\phi_{\mathrm{f}}^{\mathrm{opt}} = \pi$.

Acknowledgments

Project supported by the National Natural Science Foundation of China (Grant Nos. 12175052 and 12405010), Hangzhou Joint Fund of the Zhejiang Provincial Natural Science Foundation of China (Grant No. LHZSD24A050001), the Hangzhou Leading Youth Innovation and Entrepreneurship Team Project (Grant No. TD2024005), the HZNU scientific Research and Innovation Team Project (Grant No. TD2025003), the Guizhou Province Higher Education Teaching Content and Curriculum System Reform Project (Grant No. 2023233), the Guizhou Education Department Young Talent in Science and Technology Program (Grant Nos. QianJiaoJi[2024]174 and QianJiaoJi[2024]178), and Guizhou Provincial Theoretical Innovation Project (Grant No. GZLCLH-2025-ZX).

References

[1] Liu J, Yuan H, Lu X M and Wang X 2019 *J. Phys. A: Math. Theor.* **53** 023001
[2] PLuca P, Augusto S, Markus O K, Roman S and Philipp T 2018 *Rev. Mod. Phys.* **90** 035005
[3] Huang J H, Zhuang M and Lee C H 2024 *Appl. Phys. Rev.* **11** 031302
[4] Helstrom C 1967 *Phys. Lett. A* **25** 101
[5] Helstrom C 1968 *IEEE Trans. Inform. Theory* **14** 234
[6] Aharonov Y, Albert D Z and Vaidman L 1988 *Phys. Rev. Lett.* **60** 1351
[7] Yang J 2024 *Phys. Rev. Lett.* **132** 250802
[8] Zhang L J, Datta A and Walmsley I A 2015 *Phys. Rev. Lett.* **114** 210801
[9] Xu L, Liu Z X, Datta A, Knee G C, Lundeen J S, Lu Y Q and Zhang L J 2020 *Phys. Rev. Lett.* **125** 080501
[10] Huang J H, Hu X Y, Dada A C, Lundeen J S, Jordan K M, Chen H and An J Q 2022 *Phys. Rev. A* **106** 053704
[11] Chen G, Aharon N, Sun Y N, Zhang Z H, Zhang W H, He D Y, Tang J S, Xu X Y, Kedem Y, Li C F and Guo G C 2018 *Nat. Commun.* **9** 93
[12] Kim Y, Yoo S Y and Kim Y H 2022 *Phys. Rev. Lett.* **128** 040503
[13] Dixon P B, Starling D J, Jordan A N and Howell J C 2009 *Phys. Rev. Lett.* **102** 1351 173601
[14] Starling D J, Dixon P B, Jordan A N and Howell J C 2010 *Phys. Rev. A* **82** 063822
[15] Xu X Y, Kedem Y, Sun K, Vaidman L, Li C F and Guo G C 2013 *Phys. Rev. Lett.* **111**, 033604
[16] Huang J Z, Li Y J, Li H J and Zeng G H 2019 *Phys. Rev. A* **100** 012109
[17] Fang S Z, Dai Y, Jiang Q W, Tan H T, Li G X and Wu Q L 2021 *Chin. Phys. B* **30** 060601
[18] Xiong S J, Sun Z, Su Q P, Xi Z J, Yu L, Jin J S, Liu J M, Nori F and Yang C P 2021 *Optica* **8** 1003
[19] Sun Z, Liu J, Ma J and Wang X G 2015 2015 *Sci. Rep.* **5** 8444
[20] Sun Z, Ma J, Lu X M and Wang X G 2010 *Phys. Rev. A* **82** 022306
[21] Knee G C, Briggs G A D, Benjamin S C and Gauge E M 2013 *Phys. Rev. A* **87** 019906
[22] Song Q, Li H, Huang J, Huang P, Tan X, Tao Y, Shi C and Zeng G H 2023 *Commun. Phys.* **6** 370
[23] Qiu J D, Li Z X, Xie L G, Luo L, H Yu, Ren C G, Zhang Z Y and Du J L 2021 *Chin. Phys. B* **30** 064216
[24] Zhang M, Yu H M, Yuan H D, Wang X G, Dobrzanski R D and Liu J 2022 *Phys. Rev. Research* **4** 043057
[25] Zhong W, Sun Z, Ma J, Wang X G and Nori F 2015 2015 *Phys. Rev. A* **87** 022337
[26] Alves G B, Escher B M, Matos Filho R L, Zagury N and Davidovich L 2015 *Phys. Rev. A* **91** 062107